ACS OMEGA

http://pubs.acs.org/journal/acsodf

Article

Research on the Effect of Extinction Characteristics of Coal Dust on Visibility

Jingjing Yan, Fei Wang,* Yucheng Li, Hongwei Liu, Yabin Gao, and Ziwen Li

Cite This: *ACS Omega* 2022, 7, 28293−28303

Read Online

ACCESS | Metrics & More | Article Recommendations

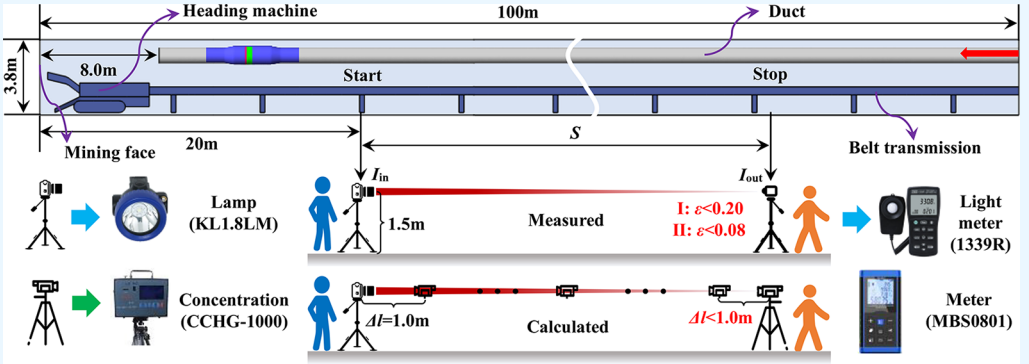

ABSTRACT: A good knowledge of the reduction mechanism of visibility is fundamental to developing preventive strategies in coal mines. In this work, the Mie theory was selected for investigating the absorption and scattering of coal dust. A prediction model for evaluating the visibility was developed based on the extinction characteristics of coal dust. The optical properties have been discussed to simplify the model and clarify the relationships among the different wavelengths and diameters. Additionally, the variety of extinction coefficients can be reasonably used in guiding the calculated visibility under different conditions. The experimental results demonstrated that the reduction of visibility was attributed to the synergistic effect of the extinction of coal dust and droplet. For the field application of this prediction model, the relative errors of the calculated and measured visibility were 9.8 and 7.1% from models I and II, which reflected the small deviation between the two methods. The prediction model can accurately describe the visibility in mines due to coal dust pollution. The exploration results provide a significant reference for the development and application of air cleaning technology for increased visibility.

1. INTRODUCTION

With the increase in coal production for sharp energy consumption, coal dust is more likely to be generated, which leads to a great risk of occupational diseases—pneumoconiosis.[1−5] Related literature revealed that the dust concentration in the main dust-producing site of coal mine can be as high as 3000−5000 mg/m^3 without no dust-prevention measures.[6] Nowadays, the use of different coal dust suppression systems and technology, including ventilation, air purification via dust collector, and dust reduction via spraying, has attracted much attention.[7−9] Despite this, the average coal dust reduction efficiencies were 73 and 82% when applied a new dust reduction technology.[10] It is challenging for mining below 4.0 (total dust) and 2.5 mg/m^3 (respirable dust) to meet the regulation of the National Health and Wellness Committee of China.[11] According to statistics, the accumulation of coal dust would seriously result in poor air circulation and reduce its visibility during working.[12] However, there are some limitations to their mechanism of coal dust and visibility, especially with regard to concentration and size distribution during tunneling.

Visibility is an important indicator of air quality that reflects the atmospheric turbidity, as demonstrated in previous research.[13,14] The degradation of visibility is a complicated issue because many factors can affect it simultaneously, including the meteorological factors (e.g., relative humidity and wind speed), composition,[15] concentrations, and size distributions of particles,[16] which in turn are subject to the influence of different ambient conditions. This is because the visibility is inversely related to extinction characteristics, which are dependent on the scattering and absorption of particles. Ma

Received: May 3, 2022
Accepted: July 25, 2022
Published: August 8, 2022

Table 1. Proximate and Ultimate Analysis of the Coal Dust Used in the Experiment[a]

	proximate analysis (wt %, d)				ultimate analysis (wt %, daf)				
sample	M_{ar}	V_d	FC_d	A_d	C_{daf}	H_{daf}	O_{diff}	N_{daf}	S_{daf}
Shanxi, China	2.77	8.45	79.94	8.84	85.15	3.18	1.83	1.15	0.82

[a]M_{ar} refers to the moisture content. A, V, and FC refer to ash, volatile, and fixed carbon content, respectively. C, H, O, N, and S represent the elements of coal dust. "diff" refers to difference; "d" and "daf" represent dry basis and dry ash-free basis, respectively. All the measurements were duplicated three times; the result in this table is the average; and the standard deviations of the quantities were less than 0.01.

et al. numerically explored the visibility by the Monte-Carlo method.[17] The results indicated that single scattering is the main factor introducing the visibility errors, and the multiple-scattering effect may be not negligible, especially for the low-visibility atmosphere. Molnár et al. found that the hygroscopic growth rate had a significant effect on the visibility under ambient RH conditions.[18] Therefore, quantifying the scattering and absorption efficiency factors of individual coal dust is critical to the understanding and modeling of the light attenuation process.

Over the past several decades, numerous studies related to the absorption and scattering of particles have been widely conducted.[19−21] Andueza et al. proposed a numerical method to investigate light scattering by particles based on the Maxwell equations.[22] Ma et al. indicated that the scattering of particles has remarkable connections with the particle complex refractive index.[23] Di Biagio et al. investigated the relationship of the refractive index and single-scattering albedo on particle content to provide a parameterization of the dust absorption as a function of its mineralogy.[24] Meanwhile, the absorption and scattering of particles are the functions of the size distribution. As Yuan et al. reported, the reduction of visibility was mainly caused by fine particles with a high scattering efficiency.[25] Zou et al. showed that $PM_{2.5}$ was negatively correlated with visibility.[26] In addition, the particle characteristic of hygroscopic growth, which is related to relative humidity (RH) has significant impacts on their optical properties. Molnár et al. indicated that the increased effect of absorption and scattering with higher ambient RH resulted in light extinction.[18] Moreover, the reduction of visibility was attributed to the increasing concentration in the ambient.[27] Zhao and Ambrose found that the extinction coefficient was linearly related to the dust concentration.[28] This is because the multiple scattering was positively related to the concentration, which raised the number of particles per unit volume. However, different patterns of scattering are distinguished by the ratio of the size of spherical particle to the wavelength, that is, $\alpha = \pi d/\lambda$. For $\alpha \ll 1$, the Rayleigh scattering approximation becomes valid. When the particle size is comparable to the wavelength of light ($\alpha \gtrsim 1$), the scattering behavior would move to the Mie regime. Geometric scattering ($\alpha \gg 1$) takes place if the interfering atmospheric particles are much larger than the wavelength of incident light.

In addition to the impacts of the particle attributes (size) and physical factors (concentrations and relative humidity), the chemical composition is also a key parameter that influences visibility. Carbonaceous particles may contribute to visibility degradation and radiative transfer through the atmosphere because of their chemical and catalytic properties.[29] Carbonaceous materials, components of coal dust, are the major contributor to the extinction process directly by its optical properties and indirectly by the refractive index.[30−32] If the coal dust was assumed to be spherical in the whole data treatment, which was currently used widely to determine the extinction coefficient. Although several studies, both experimental and theoretical,[33−35] have been conducted on the estimation of an overall extinction coefficient for visibility, there have been few studies of visibility using the calculated model. The calculation of the extinction coefficient can be roughly divided into three categories, including regression equation, IMPROVE, and Mie theory.[36−38] Compared with the summary of the above methods in Jiang et al.,[39] the Mie theory was adopted to calculate the optical parameters of coal dust based on their size distribution and the complex refractive index.

Usually, variation in concentration and size distribution control changes in the scattering and absorption efficiencies of coal dust. Despite the significant influence of particle size, the accuracy of visibility is also highly dependent on the predicted mass concentration. Thus, measuring the extinction variability is a test to understand how the optical properties vary with their temporal and spatial variability. Many studies exist in the literature that connects visibility with the atmosphere of open spaces,[26,40] but very few studies were carried out in the confined space such as mines, where the visibility has reduced rapidly and kept at the level of a few meters.[41] Noteworthy, the limitations in the field of study are mainly concerned with methods. With regard to an analysis of multiple scattering characteristics of spherical coal dust, most analogous studies on visibility are done by adopting experimental measurement and numerical simulation, out of which the numerical method is the most widely applied due to its strong operability and easy extraction of parameters.[42] In order to improve the prediction of visibility, this study proposed a calculated model.

As reviewed above, the purpose of this present work is to illustrate the prediction model of visibility in the coal mines. We first studied the absorption and scattering of coal dust based on the Mie theory. The effects of wavelength and size distribution on optical parameters were quantitatively investigated. Then, the calculated model of extinction combined with the experiment of light attenuation was adopted to further study the variation of the extinction coefficient. Furthermore, the visibility prediction model was validated by comparing the calculated and measured results with different concentrations and relative humidity. Finally, the visibility of the mine was explored according to field applications. The exploration results of this study will provide a scientific reference for the development and application of air cleaning technology for increased visibility.

2. THEORY AND METHOD

2.1. Preparation of the Coal Dust. The experimental coal samples were freshly collected from a producing coalfield area present in the province of Shanxi, China, and were utilized as a raw material of coal dust. The obtained coal samples were crushed into powder and ground to particles of ∼200 mesh. Afterward, the basic properties of coal samples were conducted using an automated industrial analyzer (TGA-200) with

https://doi.org/10.1021/acsomega.2c02739
ACS Omega 2022, 7, 28293−28303

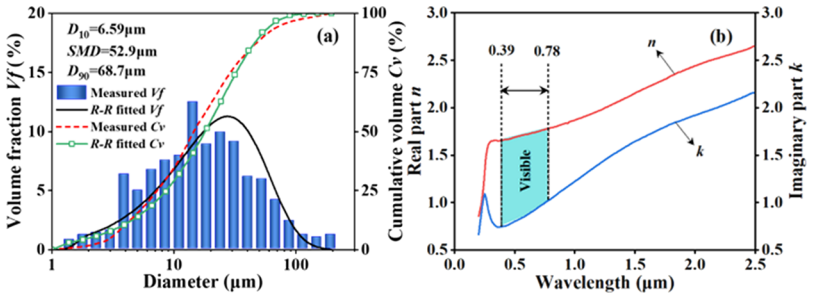

Figure 1. Coal dust characteristic parameters: (a) size distribution and (b) refractive index.

reference given to the Chinese National Standard GB/T 212-2008. The specific compositions of proximate and ultimate analysis are listed in Table 1. Then, the size distribution of coal dust was measured by a dust morphology and dispersion tester (WKL-722), as shown in Figure 1a. The refractive index of the coal dust was measured using a digital refractometer (RM 40, Mettler Toledo) within a range of 1.3200 to 1.7000 n_D and a resolution of ±0.0005, as shown in Figure 1b. Likewise, the refractive index data of air and pure water measured at a visible wavelength were m_{air} = 1.0 and m_{water} = 1.33, respectively.

2.2. The Extinction Model of Coal Dust. In this section, the finite element method coupled with the Mie theory was used to evaluate the extinction of coal dust according to size parameter α. As shown in Figure 2, when the electromagnetic

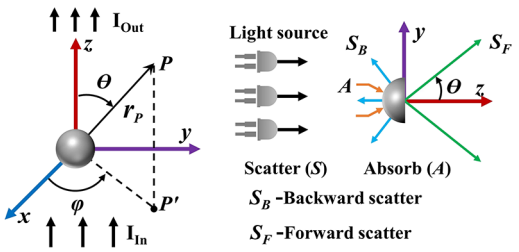

Figure 2. Extinction model of the coal dust particle.

wave was incident from the z axis of the coordinate system, the interaction with a single particle resulted in the event of extinction, where r_P represents the distance from the scattering to the observation position P and φ is the azimuth angle.

For isotropic spherical coal dust, the expression of scattered light amplitude functions can be described as[43]

$$\begin{cases} S_1(\theta) = \sum_{n=1}^{\infty} \frac{2n+1}{n(n+1)}[a_n\pi_n(\cos\theta) + b_n\tau_n(\cos\theta)] \\ S_2(\theta) = \sum_{n=1}^{\infty} \frac{2n+1}{n(n+1)}[a_n\tau_n(\cos\theta) + b_n\pi_n(\cos\theta)] \end{cases} \quad (1)$$

where θ is the scattering angle, °, τ_n and π_n are the direction-dependent functions composed of the Legendre function only determined by the scattering angle, and a_n and b_n are known as Mie coefficients, which are related to the incident wavelength and size of the coal dust. Therefore, the Mie coefficient can be expressed as follows:

$$\begin{cases} a_n = \frac{\psi_n(\alpha)\psi_n'(m\alpha) - m\psi_n'(\alpha)\psi_n(m\alpha)}{\xi_n(\alpha)\psi_n'(m\alpha) - m\xi_n'(\alpha)\psi_n(m\alpha)} \\ b_n = \frac{m\psi_n(\alpha)\psi_n'(m\alpha) - \psi_n'(\alpha)\psi_n(m\alpha)}{m\xi_n(\alpha)\psi_n'(m\alpha) - \xi_n'(\alpha)\psi_n(m\alpha)} \end{cases} \quad (2)$$

where ψ_n and ξ_n are the Ricatti−Bessel functions, $m = n + ki$ is the complex refractive index of spherical coal dust, and n and k represent real and imaginary parts, respectively. In the Mie theory, $\alpha = \pi d/\lambda$ represents the dimensionless size parameter, where λ is the wavelength of the incident light, μm, and d is the diameter of the coal dust, μm.

According to the Mie method, the absorption and scattering performance of single spherical particle should be determined before considering the extinction properties. The optical properties (i.e., extinction efficiency factor Q_{ext}, absorption efficiency factor Q_{abs}, and scattering efficiency factor Q_{sca}) can be described by the following formulas:

$$Q_{sca}(\alpha, n) = \frac{2}{\alpha^2}\sum_{n=1}^{\infty}(2n+1)(|a_n|^2 + |b_n|^2) \quad (3)$$

$$Q_{ext}(\alpha, n) = \frac{2}{\alpha^2}\sum_{n=1}^{\infty}(2n+1)\mathrm{Re}(a_n + b_n) \quad (4)$$

Based on conservation theory of extinction, the absorption efficiency factor Q_{abs} can be described as the following expression.

$$Q_{abs}(\alpha, n) = Q_{ext}(\alpha, n) - Q_{sca}(\alpha, n) \quad (5)$$

Moreover, single scattering albedo (SSA) is a commonly known parameter for evaluating the percentage of light absorption and scattering properties.[44] The SSA can be written as the ratio of the scattering efficiency factor to the extinction efficiency factor.[45]

$$SSA = \frac{Q_{sca}}{Q_{sca} + Q_{abs}} \quad (6)$$

where SSA = 0 represents purely absorbing but non-scattering. When the SSA value increases from 0.0 to 1.0, it indicates the stronger scattering in the light extinction. Furthermore, the asymmetry factor (g), which determined the amount of forward and backward scattering, was used to evaluate the scattering type as the scattering angle distribution.[46,47] The asymmetry factor varies from −1 to 1, representing the full backward scattering ($\theta \approx 180°$) to full forward scattering ($\theta \approx 0°$).[48]

2.3. Establishment of Visibility Prediction Model. A deeper understanding of how the coal dust attenuates light is

https://doi.org/10.1021/acsomega.2c02739
ACS Omega 2022, 7, 28293−28303

necessary to know how the extinction impacts visibility.[2] As shown in Figure 3, when a light beam passes through an

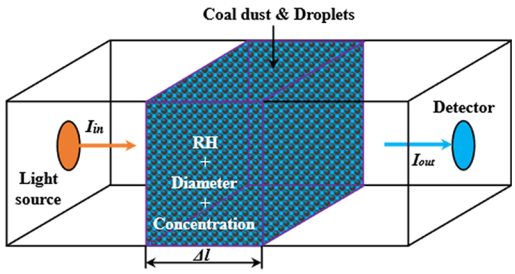

Figure 3. Light attenuation process of coal dust.

interval distance Δl of the coal dust, its incident power I_{in} attenuated to I_{out} due to scattering and absorption. The Beer–Lambert law stated that light transmitted through a mixture of coal dust and droplets will be attenuated as follows:[49]

$$I_{out} = I_{in}\exp\left(-\int_0^L B_e \mathrm{d}L\right) \tag{7}$$

where I_{in} is the incident light intensity, lx; I_{out} is the transmitted light intensity, lx, L is the extinction optical path length, m, and B_e denotes the extinction coefficient, 1/m, which represents the rate of diminution of transmitted light in response to the concentration and ambient conditions.[50] If the size distribution of coal dust follows the Rosin–Rammler (R-R) method, the expression of extinction coefficient B_e can be obtained by combining eq 4:[51]

$$B_e = \frac{\pi}{4} N \sum_{i=1}^{M} [d_i^2 Q_{ext} y_i(d)] \tag{8}$$

where Q_{ext} is the extinction efficiency factor determined by the coal dust size and wavelength of light (λ) following the Mie theory,[52] N is the coal dust number in a certain space volume, $1/m^3$, d_i is the i_{th} diameter for coal dust, m, M is the number of different coal dust diameter, $y_i(d)$ is the cumulative percentage undersize mass fraction distribution function, which is widely recognized as following:

$$y_i(d) = 1 - \exp[-(d_i/d_{mea})^n] \tag{9}$$

Here, d_{mea} represents the characteristic size corresponding to the diameter when $y_i(d) = 1 - e^{-1}$. n is the spread index of the distribution, which controls the shape of the function. If the n value is smaller, the coal dust size distribution will be wider.

According to eq 8, the extinction coefficient B_e is closely correlated with the coal dust number N. It was assumed that the mass of per unit volume of coal dust was W, mg/m^3; the relationship between the W and N can be described as follows:

$$W = \rho C_v N \sum_{i=1}^{M} [d_i^3 y_i(d)] \tag{10}$$

where ρ is the density of coal dust, 1450 mg/cm^3; C_v is the irregularity coefficient of coal dust. When $C_v = \pi/6$, the coal dust is defined as a spherical particle; d_i represents the equivalent diameter, cm.

Visibility is known as the meteorological optical range (MOR) determined by the amount of light extinction by coal dust. According to the Koschmieder's formula in eq 10, the atmospheric visibility (V) was derived by the following relationship:[17]

$$V = -\ln(\varepsilon)/\sum_{1}^{j} B_{ej} \tag{11}$$

In this formula, j represents the number of Δl along the detection length, and ε is the contrast threshold of the human eye, which is inversely proportional to the incident light intensity.[53] Previous research has shown that the visibility observation follows the Commission for Instruments and Method of Observation (CIMO) guide, which suggests that the value of ε is 0.05 in the aviation domain. However, the contrast threshold ε mainly depended on the brightness environment or lighting conditions. Consequently, the visibility can be deduced from the atmosphere extinction coefficient and light model that can be easily obtained by eq 8.

2.4. Experiment Setup and Methodology. *2.4.1. Experimental Facility.* The extinction coefficient is generally difficult to directly observe, especially the multiple-scattering effect. Moreover, significant differences have been reported in different refractive indexes and size distribution among coal dust. For this reason, it becomes necessary to study the light extinction law. Figure 4 illustrates the detailed experiment setup of the measuring system for light attenuation. The experimental device was specially designed for light intensity detection with dimensions (200 × 160 × 340 mm) and a volume of 1.5 × 10^{-3} m^3. The device mainly presented two ports to measure the concentration and relative humidity (RH)

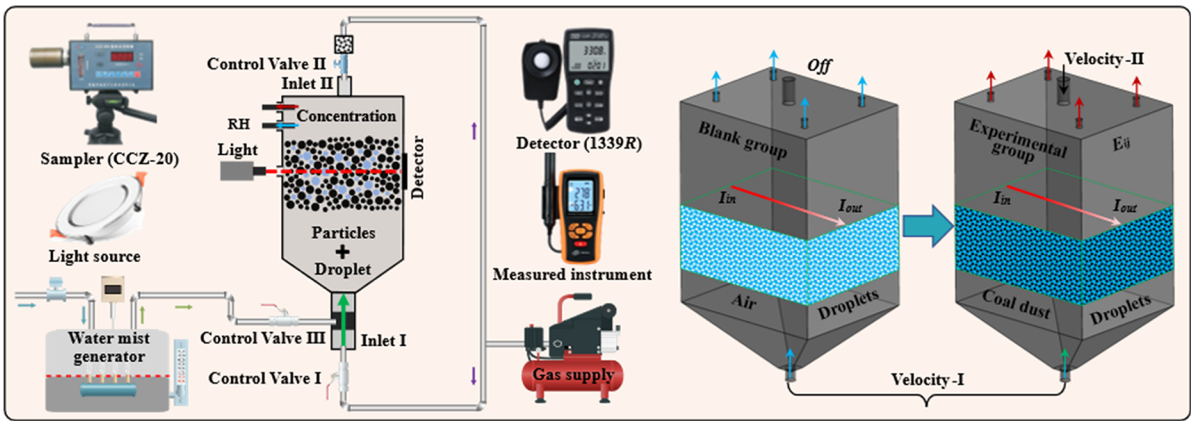

Figure 4. Diagram of the experimental setup for measuring the extinction coefficient.

https://doi.org/10.1021/acsomega.2c02739
ACS Omega 2022, 7, 28293−28303

Table 2. Scheme of the Experimental Group

	mass flow rate (mg/min)			
	7.55×10^{-2}	2.27×10^{-1}	3.78×10^{-1}	6.04×10^{-1}
	concentration (mg/m^3)			
experimental group E_{ij}	100	300	500	800
relative humidity (%)				
60	E_{11}	E_{12}	E_{13}	E_{14}
70	E_{21}	E_{22}	E_{23}	E_{24}
80	E_{31}	E_{32}	E_{33}	E_{34}
90	E_{41}	E_{42}	E_{43}	E_{44}

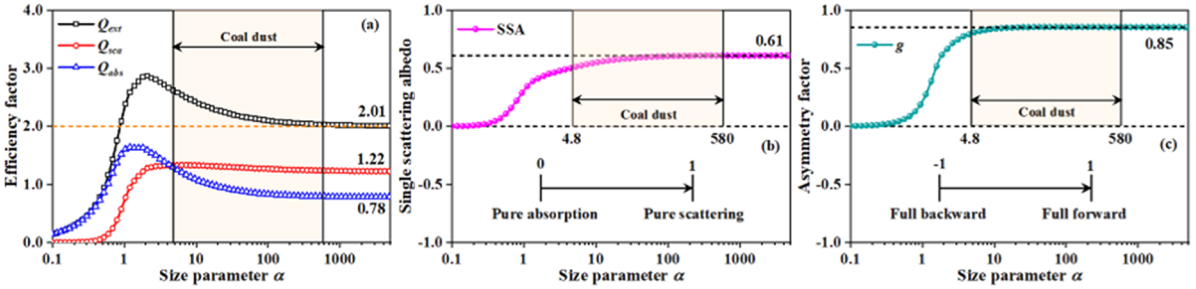

Figure 5. Optical parameters at λ = 0.65 μm. (a) Efficiency factor, (b) single scattering albedo, and (c) symmetry factor.

Table 3. Optical Parameters at d = 10.0 μm

λ (μm)	m	α	Q_{sca}	Q_{abs}	Q_{ext}	SSA	g
0.39	1.656 + 0.746i	80.5	1.2376	0.8696	2.1073	0.5873	0.8801
0.45	1.668 + 0.768i	69.8	1.2458	0.8735	2.1194	0.5878	0.8767
0.55	1.705 + 0.832i	57.1	1.2646	0.8734	2.1380	0.5915	0.8671
0.65	1.737 + 0.908i	48.3	1.2852	0.8714	2.1565	0.5960	0.8564
0.78	1.782 + 1.022i	40.3	1.3149	0.8658	2.1807	0.6030	0.8409

by the sampler (CCZ-20) and intelligent hygrometer (GM1361), respectively. A coal dust feeding chamber was placed above the equipment to provide desired intake particles. Furthermore, the relative humidity was refilled with a water mist generator through the control valve and gas supply to achieve the desired ambient condition. An LED lamp with a broad emission spectrum in the visible band from 390 to 780 nm was used as a light source. The transmitted light intensity was detected by the light meter (1339R). We have designed an experimental matrix that includes variations in both concentration and relative humidity as shown in Figure 4. An experimental group has been defined (E_{ij}) together with a RH = 60% black group, which promotes the accuracy.

2.4.2. Operating Conditions. The parameters of E_{ij} taken into consideration in this study are summarized in Table 2. In particular, the diffusion velocity was first controlled by a compression pump. If the time $t \leq 2.0$ min, the velocity I and II were set for v_1 = 2.0 m/s and v_2 = 5.0 m/s, respectively. After that, the values of v_1 = 10.0 m/s and v_2 = 3.0 m/s within 8.0 min ensure uniform mixing and prevent settlement. Meanwhile, the selected light intensity ranged from 1800 to 2400 lx for all experiments in the study. Then, the light attenuation experiments were performed as in Table 2 at an initial pressure of 101 kPa and a normal temperature of 293 K.

3. RESULTS AND DISCUSSION

3.1. Optical Properties of Coal Dust. As shown in Table 1, the higher fixed carbon FC_d and carbon element C_{daf} definitely illustrate that the components of coal dust are mainly carbonaceous material, which shows a stronger extinction ability. The optical parameters, such as efficiency factor (Q_{sca}, Q_{abs}, Q_{ext}), single scattering albedo (SSA), and symmetry factor (g), are significant to the extinction of coal dust. In this section, the optical properties have been discussed to simplify the model and clarify the relationships among the different diameters and wavelengths.

3.1.1. Effect of Diameter on the Optical Parameters. As shown in Figure 5a, the effect of diameter on optical parameters was simulated with λ = 0.65 μm. It can be observed that the efficiency factor (Q_{sca}, Q_{abs}, Q_{ext}) first increased rapidly with increasing the α in the Rayleigh regime ($\alpha \ll 1$) and then gradually decreased after reaching the geometric regime ($\alpha \gg 1$). For the coal dust sample in the Mie regime ($4.8 < \alpha < 580$), a gentle decrease between the Q_{ext} and Q_{abs} was found since the stable values of 2.01 and 0.78. However, the Q_{sca} showed an almost constant value of 1.22 as the α increases from 4.8 to 580. Accordingly, as shown in Figure 5b, the SSA slowly increased with the increase of α and then became 0.61 when $\alpha > 48.3$. In this regard, it was mainly scattering within the extinction of coal dust, which also

https://doi.org/10.1021/acsomega.2c02739
ACS Omega 2022, 7, 28293−28303

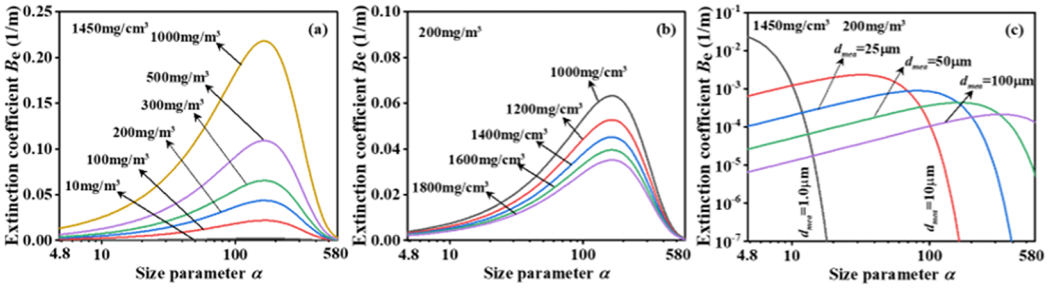

Figure 6. Effect of (a) concentration, (b) density, and (c) mean diameter on the extinction coefficient.

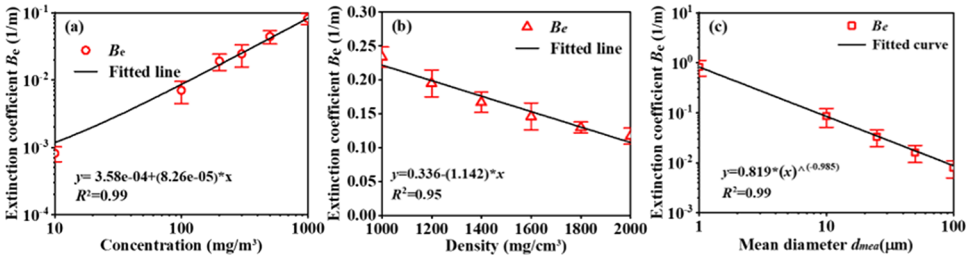

Figure 7. Fitted results of the calculated extinction coefficient. (a) Concentration, (b) density, and (c) mean diameter.

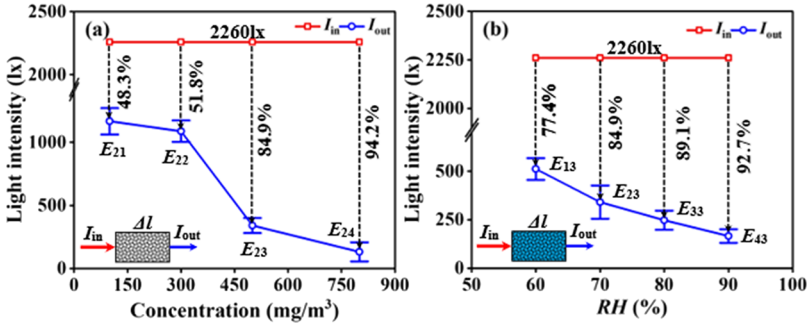

Figure 8. Variations of intensity attenuation in experiment with different (a) concentrations and (b) relative humidities.

indicated that the scattering ability can be promoted by enhancing the α. Meanwhile, it could be seen from the g in Figure 5c that the scattering light direction mainly concentrated at forward scattering ($\theta < 90°$) when $\alpha > 11.9$. That is to say, the stronger forward scattering would increase the chance of capturing light intensity by a detector in experiment. Therefore, the above results indicated that the dominant role of size distribution should be considered to improve the visibility prediction model.

3.1.2. Effect of Wavelength on the Optical Parameters. According to Figure 1b, the refractive index m of coal dust increased as the wavelength increased. Table 3 presents the results of optical variation at visible λ when $d = 10.0$ μm. It can be found that the Q_{sca} of the five incident wavelengths ranged from 1.2376 to 1.3149 due to the increase of real part n of the refractive index. Although imaginary part k increased from 0.746 to 1.022, the Q_{abs} indicated a trend of first increasing and then decreasing. However, the Q_{ext} had a linear growth relationship with higher $R^2 = 0.99$ as λ increases in the Mie regime. The reason for this phenomenon is that the α decreases from 80.5 to 40.3, which is very much dependent on λ as the Mie theory under same size of coal dust. From the comparison of the results of Dillner et al. and Xia et al., Q_{ext} decreases with increasing α, and light wavelength has a lesser effect on the Q_{ext} value of larger particles.[54,55] In contrast to the weak increase of SSA, the decreasing of g indicated that the extinction of coal dust shows more scattering dependence with increasing λ. This is mainly due to the fact that forward scattering promotes the extinction effect.

3.2. Variation of the Extinction Coefficient. Figure 6 illustrates the change of the extinction coefficient under different concentrations, densities, and mean diameters. As shown in Figure 6a,b, the signal peak distribution of B_e was observed as the increasing diameter which followed the *R-R* with d_{mea} = 49.6 μm and n = 1.8 in Figure 1a. It can be evidently found that for a given ρ = 1450 mg/cm^3, the calculated B_e would be much greater with the increase the concentration from 10 to 1000 mg/m^3. Furthermore, the higher concentration corresponding to increasing N enhanced the multiple scattering effect, which lead to broadening the peaks of B_e. A similar variation tendency could also be observed in the cases with W = 200 mg/m^3. With increasing the density, the decrease in the N would definitely restrain the extinction of coal dust.

As analyzed above, size distribution played a key role in the variation of the Q_{ext}; accordingly, the significant effects of the mean diameter (d_{mea}) on B_e are shown in Figure 6c. When d_{mea} decreased from 100 to 1.0 μm, the peak value of B_e was promoted about 99.1 times, which was beneficial to the dramatic increase of the N. Hence, it was found that the

https://doi.org/10.1021/acsomega.2c02739
ACS Omega 2022, 7, 28293−28303

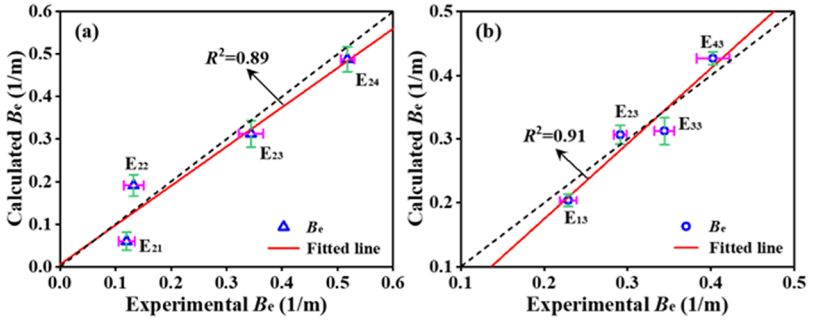

Figure 9. Comparison of experimental and calculated extinction coefficients. (a) Concentration and (b) relative humidity.

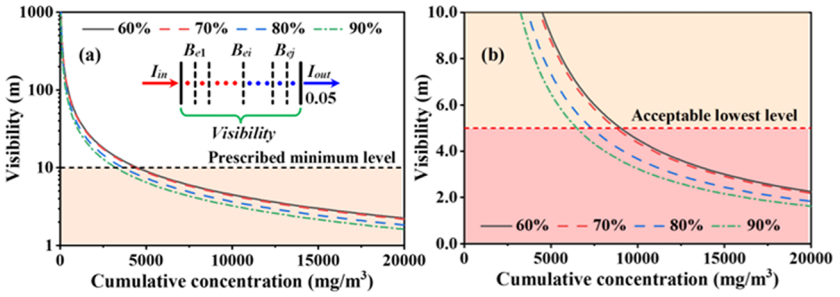

Figure 10. Variations of the calculated visibility. (a) Prescribed minimum level; (b) acceptable lowest level.

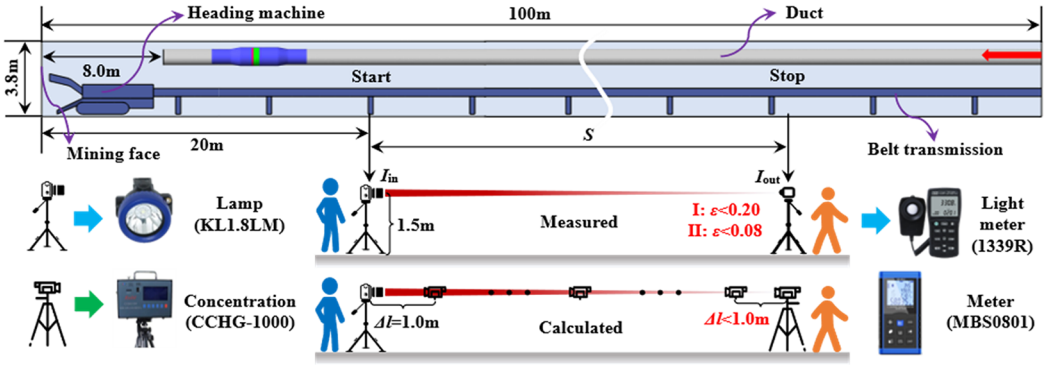

Figure 11. Layout of field applications with two methods.

variation of the extinction coefficient was determined by the physical characteristics and optical properties of coal dust.

To further study the above analysis, the fitted results about the effect of W, ρ, and d_{mea} on the calculated B_e are depicted in Figure 7. As can be seen in Figure 7a, the value for B_e clearly followed a linear relationship with the increase of coal dust W. The correlation coefficient R^2 = 0.99 indicated that the fitted formula can be adopted to predict the B_e. Zhao et al. observed a similar relationship between the B_e and concentration. They believed that the calculated B_e value was lower than the measured one due to the heterogeneity of the dust.[28] Similarly, the R^2 = 0.95 value was obtained from the linear regression model between B_e and the density of coal dust in Figure 7b. It can be seen that there was a negative correlation between B_e and ρ. Figure 7c presents the fitting curve for B_e under different mean diameter conditions. The power function and higher R^2 = 0.99 provided stronger evidence about the effect of size distribution on the calculated B_e. Therefore, we can reasonably calculate the extinction coefficient under different conditions for predicting the visibility in the experiments.

3.3. Validation of the Visibility Prediction Model. For the purpose of validating the effect of B_e on visibility, the experiments of intensity attenuation were first carried out coupled with eq 7. As shown in Figure 8a, it can be observed that the incident light intensity I_{out} gradually decreased from 48.3 to 51.8% with increasing the concentration at RH = 70%. After coal dust was further added, the transmitted light intensity I_{out} showed a significant decline of 94.2% compared with 15.3% of the blank experiment. In addition, the attenuation rate I_{out}/I_{in} of Figure 8b presented an increasing tendency with higher RH among the E_{13}, E_{23}, E_{33}, and E_{43}. Note that here, when the relative humidity is extremely high (that is, RH = 90%), the I_{out}/I_{in} = 92.7% would achieve the same extinction level at 800 mg/m^3. This is because the droplets of ambient increased with the increase of RH from 60 to 90%, which resulted in stronger scattering.[56] Hence, the effect of ambient RH and the concentration of coal dust on the visibility were evident.

With the aim of exploring the variations of intensity, the experimental B_e with different concentrations and relative humidity was calculated for evaluating the visibility model. Figure 9 demonstrates the comparison of B_e with regard to different conditions. It can be seen that the B_e calculated by eq 8 agreed well with the experimental results, and the maximum

https://doi.org/10.1021/acsomega.2c02739
ACS Omega 2022, 7, 28293−28303

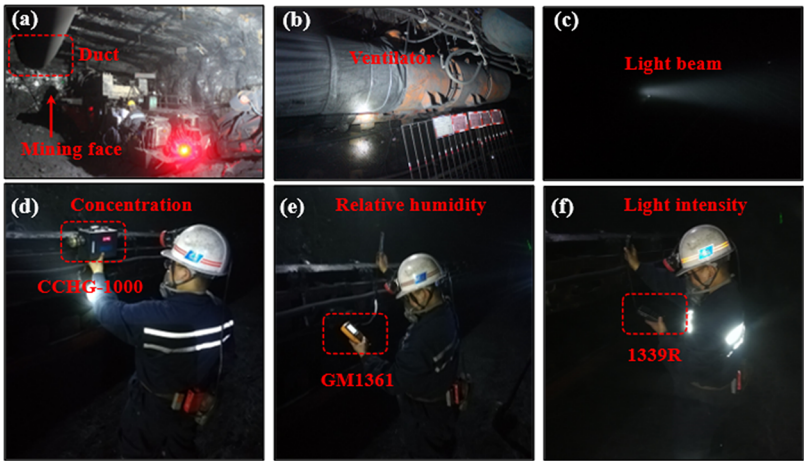

Figure 12. Arrangement of the various measuring tools used in the coal mine. (a) Ming face; (b) ventilator; (c) light beam; (d) concentration; (e) relative humidity; (f) light intensity.

relative error was less than 10%. The correlation coefficient R^2 of fitted lines was larger than 0.85, which explained that the accuracy of fitted data was effective within the experiment error. Thus, these results also indicated that the established prediction model can describe the extinction behavior of coal dust with different RH values.

According to the eq 11, the variations of the calculated visibility with different cumulative W and RH are presented in Figure 10. As shown in Figure 10a, the visibility decreased exponentially from 1000 m to a prescribed minimum level (10.0 m) with an increase in cumulative W from 65 to 4350 mg/m^3 when RH = 70%. Moreover, all the curves indicated that the range of visibility variation show a negative decline tendency as the ambient RH increases from 60 to 90%. In addition, it was noted that the visibility within 10.0 m exhibited a gradual decrease as cumulative W increased in Figure 10b. However, in the case of visibility below the acceptable lowest level (5.0 m), it was more difficult to distinguish things around us. This phenomenon indicated that the reduction of visibility was attributed to the synergistic effect of the extinction of coal dust and droplet.

3.4. Field Application and Model Verification. In order to validate the accuracy of the prediction visibility, the established model of coal dust under different relative humidities was then applied in the no. 5304 fully mechanized working face of *Changping Mine*. Figure 11 exhibits the layout of field applications with two methods to evaluate the atmospheric visibility. The pressure air quantity was measured to be 875m^3/min with a temperature of 288 K and a relative humidity of 85%. The mine headlamp with two lighting modes (I:925 lx and II:1480 lx) was arranged at a distance of 20 m from the mining face and a height of 1.5 m above the ground. Meanwhile, the size distribution of suspended coal dust was collected and then measured in the laboratory. According to eq 9, the measured data was fitted with d_{mea} = 38.4 μm and n = 1.6, which were used in the prediction model for calculated visibility V_c.

Figure 12 displays the arrangement of the various measuring tools used in field application. The main measured steps are as follows: (1) the measured lamp was installed on the tripod, and the lighting model I was chosen first. (2) The light meter (1339R) was turned on, and the detector was operated until the contrast threshold ε satisfied the requirement. Subsequently, the distance S_i measured by a laser instrument (MBS0801) was recorded for the measured visibility V_m. (3) The concentrations were measured sequentially by an instrument (CCHG-1000) at an interval distance Δl = 1.0 m from the start position. At each measured position, coal dust concentration was measured 3 times for averaging. If the distance between the measured and stop positions was lower than 1.0 m, the obtained data from each measure were used to calculate visibility V_c. (4) The lighting model was changed to II, and steps (2) and (3) were repeated to further investigate the various visibilities in the mine.

Table 4 shows the measured distance S with different light models. Mishra and Ahuja demonstrated that the visibility was determined by the contrast threshold ε in different brightness levels.[57] As seen from the data, the contrast threshold ε values for model I (925 lx) and model II (1480 lx) were measured at about 0.20 and 0.08 based on the light power.[58] The average distance S values were 8.2 and 11.3 m, which indicated that the measured number j values for the prediction model were 8 and 11 based on the interval distance Δl.

Table 4. Measured Distance with Different Light Models

name	ε	S_1/m	S_2/m	S_3/m	average/m	relative error/%
model I	0.20	8.3	7.7	8.6	8.2	6.1
model II	0.08	11.8	11.5	10.7	11.3	5.3

Tables 5 and 6 display the measured concentration and extinction coefficient in the different light models for calculated visibility. It can be clearly seen that the measured W decreased with increased distance from the start position. Combining the linear relationship between W and B_e in Figure 8, the B_e in each Δl decreased from 0.046807 to 0.013688 when j = 1 to j = 8. Similarly, when the light model was adjusted to II, the average W decreased from 503 to 83 mg/m^3, resulting in the B_e declining to7954 at j = 11.

As discussed above, the average distance S has been adopted to represent the measured visibility V_m due to its higher accuracy. In addition, the calculated visibility V_c was obtained by combining eq 8 with the total extinction coefficient in Tables 5 and 6. The comparison of the V_m and V_c is shown in Table 7. It can be found that the relative errors of the V_m and V_c were 9.8 and 7.1% from models I and II, which reflected the small deviation between the two methods. Accordingly, within

https://doi.org/10.1021/acsomega.2c02739
ACS Omega 2022, 7, 28293−28303

Table 5. Measured Concentration and Extinction Coefficient in the Light Model I

	concentration (mg/m^3)				
model I	measured 1	measured 2	measured 3	average	B_e (1/m)
j = 1	506	487	475	489	0.046807
j = 2	384	394	408	395	0.037809
j = 3	344	358	332	345	0.033023
j = 4	307	295	284	295	0.028237
j = 5	277	253	268	266	0.025462
j = 6	209	225	238	224	0.021441
j = 7	197	208	189	198	0.018953
j = 8	134		151	143	0.013688
total	2453	2210	2260	2308	0.225421

Table 6. Measured Concentration and Extinction Coefficient in the Light Model II

	concentration (mg/m^3)				
model II	measured 1	measured 2	measured 3	average	B_e (1/m)
j = 1	504	482	523	503	0.048147
j = 2	408	426	419	418	0.039979
j = 3	316	347	327	330	0.031588
j = 4	294	277	286	286	0.027344
j = 5	244	253	231	243	0.023228
j = 6	206	197	209	204	0.019527
j = 7	189	195	204	196	0.018761
j = 8	151	132	122	135	0.012922
j = 9	115	108	94	106	0.010105
j = 10	90	99	84	91	0.08723
j = 11	71	92		83	0.07954
total	2588	2608	2585	2594	0.248279

Table 7. Comparison of the Measured and Calculated Visibilities

name	V_m (m)	V_c (m)	relative error
model I	8.2	7.4	9.8%
model II	11.3	12.1	7.1%

the acceptable limit error of 10%, it can be conducted that the prediction model can accurately describe the visibility in mines due to particle pollution.

4. CONCLUSIONS

In this study, the Mie theory was selected for investigating the absorption and scattering of coal dust. A prediction model for evaluating the visibility of coal dust was developed based on the Beer−Lambert law and Koschmieder's formula. The effects of extinction characteristics of coal dust on visibility were systematically analyzed. The main conclusions obtained are summarized as follows:

(1) The significant various optical parameters were observed with the increasing size parameter of coal dust at λ = 0.65 μm. Also, the scattering ability and type in extinction were promoted by increasing the diameter according to the SSA and symmetry factor. However, the extinction efficiency factor slightly varied when the incident wavelength ranged from 0.39 to 0.78 μm for a certain diameter.

(2) The relationship of the coal dust number and concentration was first illustrated for the calculated extinction coefficient. In general, the value of the extinction coefficient clearly followed the linear relationship with increasing concentration. A significant negative correlation was found between the extinction coefficient and density based on their linear regression model. The higher correlation coefficient provided stronger evidence about the effect of size distribution on the extinction coefficient.

(3) Based on the experiment of intensity attenuation, the calculated extinction coefficient agreed well with the experimental results at different concentrations and relative humidity. The visibility decreased exponentially with the increase in cumulative concentration. Moreover, the range of visibility presented a negative decline tendency as the relative humidity increased from 60 to 90%. Thus, these results indicated that the reduction of visibility was attributed to the synergistic effect of the extinction of coal dust and droplet.

(4) For the field application of this prediction model, the relative errors of the calculated and measured visibility were 9.8 and 7.1% from models I and II, which reflected the small deviation between the two methods. The prediction model can accurately describe the visibility in mines due to particle pollution.

AUTHOR INFORMATION

Corresponding Author

Fei Wang − *College of Safety and Emergency Management Engineering and Center of Shanxi Mine Safety for Graduate Education Innovation, Taiyuan University of Technology, Taiyuan 030024, P.R. China;* orcid.org/0000-0003-2943-5553; Email: tyutwangfei@126.com

Authors

Jingjing Yan − *College of Safety and Emergency Management Engineering and Center of Shanxi Mine Safety for Graduate Education Innovation, Taiyuan University of Technology, Taiyuan 030024, P.R. China;* orcid.org/0000-0002-5562-0181

Yucheng Li − *College of Safety and Emergency Management Engineering, Taiyuan University of Technology, Taiyuan 030024, P.R. China*

Hongwei Liu − *College of Safety and Emergency Management Engineering and Center of Shanxi Mine Safety for Graduate Education Innovation, Taiyuan University of Technology, Taiyuan 030024, P.R. China*

Yabin Gao − *College of Safety and Emergency Management Engineering, Taiyuan University of Technology, Taiyuan 030024, P.R. China*

Ziwen Li − *College of Safety and Emergency Management Engineering, Taiyuan University of Technology, Taiyuan 030024, P.R. China*

Complete contact information is available at: https://pubs.acs.org/10.1021/acsomega.2c02739

Notes

The authors declare no competing financial interest.

ACKNOWLEDGMENTS

This research project was funded by the Key Research and Development (R&D) Projects of Shanxi Province (no. 201803D31053); Major Technological Research Projects of Shanxi Coking Coal Group Co. Ltd. (no. 201812xs06);

https://doi.org/10.1021/acsomega.2c02739
ACS Omega 2022, 7, 28293−28303

Opening Project of State Key Laboratory of Explosion Science and Technology, Beijing Institute of Technology (KFJJ19-03 M); and National Natural Science Foundation of China (nos. 52004176 and 51774168). The authors would particularly like to express their gratitude for the scholarship from the China Scholarship Council (201906930017) and the support by Shanxi Province education innovation project for graduates (RC1900001671).

REFERENCES

(1) Cai, P.; Nie, W.; Chen, D.; Yang, S.; Liu, Z. Effect of air flowrate on pollutant dispersion pattern of coal dust particles at fully mechanized mining face based on numerical simulation. *Fuel* **2019**, *239*, 623−635.
(2) Camino, C.; Cuevas, E.; Basart, S.; Alonso-Pérez, S.; Baldasano, J. M.; Terradellas, E.; Marticorena, B.; Rodríguez, S.; Berjón, A. An empirical equation to estimate mineral dust concentrations from visibility observations in Northern Africa. *Aeolian Res.* **2015**, *16*, 55−68.
(3) Mahowald, N. M.; Ballantine, J. A.; Feddema, J.; Ramankutty, N. Global trends in visibility: implications for dust sources. *Atmos. Chem. Phys.* **2007**, *7*, 3309−3339.
(4) Wang, H.; Nie, W.; Zhang, H.; Jin, H.; Bao, Q.; Yan, J.; Liu, Q. A Synthesis of a Dust Suppressant Using the Cellulose Extracted from Maize Straw. *Starch - Starke* **2019**, *72*, DOI: 10.1002/star.201900187.
(5) Xiu, Z.; Nie, W.; Yan, J.; Chen, D.; Cai, P.; Liu, Q.; Du, T.; Yang, B. Numerical simulation study on dust pollution characteristics and optimal dust control air flow rates during coal mine production. *J. Cleaner Prod.* **2020**, *248*, No. 119197.
(6) Zhou, G.; Zhang, Q.; Bai, R.; Fan, T.; Wang, G. The diffusion behavior law of respirable dust at fully mechanized caving face in coal mine: CFD numerical simulation and engineering application. *Process Saf. Environ. Prot.* **2017**, *106*, 117−128.
(7) Geng, F.; Luo, G.; Zhou, F.; Zhao, P.; Ma, L.; Chai, H.; Zhang, T. Numerical investigation of dust dispersion in a coal roadway with hybrid ventilation system. *Powder Technol.* **2017**, *313*, 260−271.
(8) Lu, X.; Wang, D.; Xu, C.; Zhu, C.; Shen, W. Experimental investigation and field application of foam used for suppressing roadheader cutting hard rock in underground tunneling. *Tunnelling and Underground Space Technology* **2015**, *49*, 1−8.
(9) Toraño, J.; Torno, S.; Menéndez, M.; Gent, M. Auxiliary ventilation in mining roadways driven with roadheaders: Validated CFD modelling of dust behaviour. *Tunnelling and Underground Space Technology* **2011**, *26*, 201−210.
(10) Nie, W.; Yang, B.; Du, T.; Peng, H.; Zhang, X.; Zhang, Y. Dynamic dispersion and high-rise release of coal dust in the working surface of a large-scale mine and application of a new wet dust reduction technology. *J. Cleaner Prod.* **2022**, *351*, No. 131356.
(11) Han, H.; Wang, P.; Li, Y.; Liu, R.; Tian, C. Effect of water supply pressure on atomization characteristics and dust-reduction efficiency of internal mixing air atomizing nozzle. *Adv. Powder Technol.* **2020**, *31*, 252−268.
(12) Masto, R. E.; George, J.; Rout, T. K.; Ram, L. C. Multi element exposure risk from soil and dust in a coal industrial area. *J. Geochem. Explor.* **2017**, *176*, 100−107.
(13) Husar, R. B.; Holloway, J. M.; Patterson, D. E.; Wilson, W. E. Spatial and temporal pattern of eastern U.S. haziness: A summary. *Atmos. Environ.* **1981**, *15*, 1919−1928.
(14) Ghude, S.; Bhat, G.; Prabha, T.; Jenamani, R.; Chate, D.; Safai, P.; Karipot, A.; Konwar, M.; Pithani, P.; Sinha, V.; Pasumarti, R.; Dixit, S.; Tiwari, S.; Todekar, K.; Varpe, S.; Srivastava, A.; Bisht, D.; Murugavel, P.; Ali, K.; Rajeevan, M. Winter Fog Experiment Over the Indo-Gangetic Plains of India. *Curr. Sci.* **2017**, *112*, 767.
(15) Yu, X.; Ma, J.; An, J.; Yuan, L.; Zhu, B.; Liu, D.; Wang, J.; Yang, Y.; Cui, H. Impacts of meteorological condition and aerosol chemical compositions on visibility impairment in Nanjing, China. *J. Cleaner Prod.* **2016**, *131*, 112−120.
(16) Deng, X.; Tie, X.; Wu, D.; Zhou, X.; Bi, X.; Tan, H.; Li, F.; Jiang, C. Long-term trend of visibility and its characterizations in the Pearl River Delta (PRD) region, China. *Atmos. Environ.* **2008**, *42*, 1424−1435.
(17) Ma, Y.; Liu, W.; Gao, H.; Chen, N.; Xiong, X. The scattering effects on the visibility measurements of laser transmissometer in rain and fog. *Optik* **2018**, *157*, 957−967.
(18) Molnár, A.; Imre, K.; Ferenczi, Z.; Kiss, G.; Gelencsér, A. Aerosol hygroscopicity: Hygroscopic growth proxy based on visibility for low-cost PM monitoring. *Atmos. Res.* **2020**, *236*, No. 104815.
(19) Jeong, S. Y.; Chen, C.; Ranjan, D.; Loutzenhiser, P. G.; Zhang, Z. M. Measurements of scattering and absorption properties of submillimeter bauxite and silica particles. *J. Quant. Spectrosc. Radiat. Transfer* **2021**, *276*, No. 107923.
(20) Gopal, K. R.; Balakrishnaiah, G.; Arafath, S. M.; Reddy, K. R. O.; Reddy, N. S. K.; Kumari, S. P.; Kumar, K. R.; Rao, T. C.; Reddy, T. L.; Reddy, R. R.; Hussain, S. N. Measurements of scattering and absorption properties of surface aerosols at a semi-arid site, Anantapur. *Atmos. Res.* **2017**, *183*, 84−93.
(21) Li, Y.; Zhou, Y.; Sun, Z.; Gu, H.; Ma, Q.; Diao, H. Analysis of hygroscopic growth properties of soluble aerosol under severe nuclear accidents conditions. *Prog. Nucl. Energy* **2020**, *127*, No. 103464.
(22) Andueza, A.; Morales, P.; Sevilla, J. Photonic band effect in single-layers of high refractive index spheres of different compactness. *J. Appl. Phys.* **2012**, *111*, 2059.
(23) Ma, L. X.; Tan, J. Y.; Zhao, J. M.; Wang, F. Q.; Wang, C. A.; Wang, Y. Y. Dependent scattering and absorption by densely packed discrete spherical particles: Effects of complex refractive index. *J. Quant. Spectrosc. Radiat. Transfer* **2017**, *196*, 94−102.
(24) Di Biagio, C.; Formenti, P.; Balkanski, Y.; Caponi, L.; Cazaunau, M.; Pangui, E.; Journet, E.; Nowak, S.; Andreae, M. O.; Kandler, K.; Saeed, T.; Piketh, S.; Seibert, D.; Williams, E.; Doussin, J. F. Complex refractive indices and single-scattering albedo of global dust aerosols in the shortwave spectrum and relationship to size and iron content. *Atmos. Chem. Phys.* **2019**, *19*, 15503−15531.
(25) Yuan, C.-S.; Lee, C.-G.; Liu, S.-H.; Chang, J. C.; Yuan, C.; Yang, H.-Y. Correlation of atmospheric visibility with chemical composition of Kaohsiung aerosols. *Atmos. Res.* **2006**, *82*, 663−679.
(26) Zou, J.; Liu, Z.; Hu, B.; Huang, X.; Wen, T.; Ji, D.; Liu, J.; Yang, Y.; Yao, Q.; Wang, Y. Aerosol chemical compositions in the North China Plain and the impact on the visibility in Beijing and Tianjin. *Atmos. Res.* **2018**, *201*, 235−246.
(27) Xu, R. Light scattering: A review of particle characterization applications. *Particuology* **2015**, *18*, 11−21.
(28) Zhao, Y.; Ambrose, R. P. K. A real-time method for sensing suspended dust concentration from the light extinction coefficient. *J. Loss Prev. Process Ind.* **2020**, *67*, No. 104242.
(29) Penner, J. E.; Novakov, T. Carbonaceous particles in the atmosphere: A historical perspective to the Fifth International Conference on Carbonaceous Particles in the Atmosphere. *J. Geophys. Res.: Atmos.* **1996**, *101*, 19373−19378.
(30) Pauraite, J.; Minderytė, A.; Dudoitis, V.; Plauškaitė, K.; Byčenkienė, S. Effect of urban submicron particles on single scattering albedo: the case study of high pollution event. *J. Quant. Spectrosc. Radiat. Transfer* **2022**, *280*, No. 108075.
(31) Xiao, S.; Wang, Q. Y.; Cao, J. J.; Huang, R. J.; Chen, W. D.; Han, Y. M.; Xu, H. M.; Liu, S. X.; Zhou, Y. Q.; Wang, P.; Zhang, J. Q.; Zhan, C. L. Long-term trends in visibility and impacts of aerosol composition on visibility impairment in Baoji, China. *Atmos. Res.* **2014**, *149*, 88−95.
(32) Ayers, G. P.; Gras, J. L. Seasonal relationship between cloud condensation nuclei and aerosol methanesulphonate in marine air. *Nature* **1991**, *353*, 834−835.
(33) Osinga, T.; Lipinski, W.; Guillot, E.; Olalde, G.; Steinfeld, A. Experimental Determination of the Extinction Coefficient for a Packed-Bed Particulate Medium. *Exp. Heat Transfer* **2006**, *19*, 69−79.
(34) Yu, W. W.; Qu, L.; Guo, W.; Peng, X. Experimental Determination of the Extinction Coefficient of CdTe, CdSe and CdS Nanocrystals. *Chem. Mater.* **2004**, *16*, 560−560.

https://doi.org/10.1021/acsomega.2c02739
ACS Omega 2022, 7, 28293−28303

(35) Jung, C. H.; Kim, Y. P. Theoretical study on the change of the particle extinction coefficient during the aerosol dynamic processes. *J. Aerosol Sci.* **2008**, *39*, 904−916.
(36) Peng, Y.; Wang, H.; Hou, M.; Jiang, T.; Zhang, M.; Zhao, T.; Che, H. Improved method of visibility parameterization focusing on high humidity and aerosol concentrations during fog−haze events: Application in the GRAPES_CAUCE model in Jing-Jin-Ji, China. *Atmos. Environ.* **2020**, *222*, 117139.
(37) Mie, G. Beiträge zur Optik trüber Medien, speziell kolloidaler Metallösungen. *Ann. Phys.* **1908**, *330*, 377−445.
(38) Watson, J. Visibility: Science and Regulation. *J. Air Waste Manage. Assoc.* **2002**, *52*, 628−713.
(39) Jiang, L.; Zhang, Z.; Zhu, B.; Shen, Y.; Wang, H.; Shi, S.; Sha, D. Comparison of parameterizations for the atmospheric extinction coefficient in Lin'an, China. *Sci. Total Environ.* **2018**, *621*, 507−515.
(40) Verma, S.; Pani, S. K.; Kumar, D. B.; Faruqi, A. R.; Bhanja, S. N.; Mandal, M. Aerosol extinction properties over coastal West Bengal Gangetic plain under inter-seasonal and sea breeze influenced transport processes. *Atmos. Res.* **2016**, *167*, 224−236.
(41) Guo, Q.; Ren, W.; Shi, J. Foam for coal dust suppression during underground coal mine tunneling. *Tunnelling and Underground Space Technology* **2019**, *89*, 170−178.
(42) Ren, Y. H.; Qin, Y. P. Study on Contraction of Dust Control System in Continuous Coal Mining. *Adv. Mater. Res.* **2013**, *734-737*, 824−827.
(43) Zhang, Y.-G.; Zhang, J.; Wu, S.-T.; Gao, J.-L.; Hao, Z.-Q.; Li, C.-L. Study on laser scattering depolarization characteristics of typical aerosol particles. *Opt. Commun.* **2022**, *516*, No. 128183.
(44) Pokhrel, R.; Wagner, N.; Langridge, J.; Lack, D.; Jayarathne, T.; Stone, E.; Stockwell, C.; Yokelson, R.; Murphy, S. Parameterization of single-scattering albedo (SSA) and absorption Ångström exponent (AAE) with EC / OC for aerosol emissions from biomass burning. *Atmos. Chem. Phys.* **2016**, *16*, 9549−9561.
(45) Moosmüller, H.; Sorensen, C. M. Single scattering albedo of homogeneous, spherical particles in the transition regime. *J. Quant. Spectrosc. Radiat. Transfer* **2018**, *219*, 333−338.
(46) Pandolfi, M.; Ripoll, A.; Querol, X.; Alastuey, A. Climatology of aerosol optical properties and black carbon mass absorption cross section at a remote high-altitude site in the western Mediterranean Basin. *Atmos. Chem. Phys.* **2014**, *14*, 3777−3814.
(47) Enekwizu, O.; Singh, D.; Khalizov, A. Absorption and scattering of light by soot aggregates with uniform and pendular ring coatings. *J. Aerosol Sci.* **2020**, *147*, No. 105583.
(48) Barreto, G.; Canhoto, P.; Collares-Pereira, M. Combined experimental and numerical determination of the asymmetry factor of scattering phase functions in porous volumetric solar receivers. *Sol. Energy Mater. Sol. Cells* **2020**, *206*, No. 110327.
(49) Ghosh, S.; Ray, R.; Vadali, S. R.; Shome, S., *Light-Particle Interaction in Underwater: A Modified PSF*. International Conference on Communication and Signal Processing,: 2014.
(50) Xingcai, L.; Kun, N. Effectively predict the solar radiation transmittance of dusty photovoltaic panels through Lambert-Beer law. *Renewable Energy* **2018**, *123*, 634−638.
(51) Jis, A.; Ssy, A.; Ig, B.; Khc, C.; Bgk, D. Development of a new visibility parameterization based on the measurement of fog microphysics at a mountain site in Korea. *Atmos. Res.* **2019**, *229*, 115−126.
(52) Hergert, W. In *The Mie theory. Basics and applications*, International Water Management Institute, 2012.
(53) Parent, G.; Gasparotto, T.; Morlon, R.; Boulet, P. A model to assess visibility in scattering environments. *Fire Safety J* **2020**, *112*, No. 102970.
(54) Xia, Y.; Tao, J.; Zhang, L.; Zhang, R.; Li, S.; Wu, Y.; Cao, J.; Wang, X.; Ma, Q.; Xiong, Z. Impact of size distributions of major chemical components in fine particles on light extinction in urban Guangzhou. *Sci. Total Environ.* **2017**, *587-588*, 240−247.
(55) Dillner, A. M.; Stein, C.; Larson, S. M.; Hitzenberger, R. Measuring the Mass Extinction Efficiency of Elemental Carbon in Rural Aerosol. *Aerosol Sci. Technol.* **2001**, *35*, 1009−1021.
(56) Liu, X.; Gu, J.; Li, Y.; Cheng, Y.; Qu, Y.; Han, T.; Wang, J.; Tian, H.; Chen, J.; Zhang, Y. Increase of aerosol scattering by hygroscopic growth: Observation, modeling, and implications on visibility. *Atmos. Res.* **2013**, *132-133*, 91−101.
(57) Mishra, S.; Ahuja, B. Optical parameters testing to redefine visibility for low cost transmissometer using channel modeling. *Optik* **2016**, *127*, 11326−11335.
(58) Ann-Katherine, G. C.; Hilde, B.; Dirk, V.; Chantal Van, O.; Geert, S.; Frank, R.; Guy, M. In *Threshold contrast visibility of microcalcifications in digital mammography*, Proc.SPIE, 2004.

https://doi.org/10.1021/acsomega.2c02739
ACS Omega 2022, 7, 28293−28303